

# Eigenstate thermalization hypothesis and its deviations from random-matrix theory beyond the thermalization time

Jiaozi Wang,<sup>1,\*</sup> Mats H. Lamann,<sup>1</sup> Jonas Richter,<sup>2</sup> Robin Steinigeweg,<sup>1</sup> Anatoly Dymarsky,<sup>3,4,5</sup> and Jochen Gemmer<sup>1,†</sup>

<sup>1</sup>*Department of Physics, University of Osnabrück, D-49069 Osnabrück, Germany*

<sup>2</sup>*Department of Physics and Astronomy, University College London, Gower Street, London WC1E 6BT, UK*

<sup>3</sup>*Moscow Institute of Physics and Technology, 9 Institutskiy pereulok, Dolgoprudny, Russia*

<sup>4</sup>*Skolkovo Institute of Science and Technology, Skolkovo Innovation Center, Moscow, Russia*

<sup>5</sup>*Department of Physics, University of Kentucky, Lexington, Kentucky, USA*

The Eigenstate Thermalization Hypothesis (ETH) explains emergence of the thermodynamic equilibrium by assuming a particular structure of observable's matrix elements in the energy eigenbasis. Schematically, it postulates that off-diagonal matrix elements are random numbers and the observables can be described by Random Matrix Theory (RMT). To what extent physical operators can be described by RMT, more precisely at which energy scale strict RMT description applies, is however not fully understood. We study this issue by introducing a novel numerical approach to probe correlations between matrix elements for Hilbert-space dimensions beyond those accessible for exact diagonalization. Our analysis is based on the evaluation of higher moments of operator submatrices, defined within energy windows of varying width. Considering nonintegrable quantum spin chains, we observe that genuine RMT behavior is absent even for narrow energy windows corresponding to time scales of the order of thermalization time  $\tau_{\text{th}}$  of the respective observables. We also demonstrate that residual correlations between matrix elements are reflected in the dynamics of out-of-time-ordered correlation functions.

*Introduction.* In the overwhelming majority of cases, isolated quantum many-body systems undergoing unitary time evolution are expected to reach thermal equilibrium at sufficiently long times [1–5]. During the thermalization process, local memory of the initial out-of-equilibrium state is lost and observables reach a constant value that agrees with an appropriate thermodynamic ensemble average, as observed experimentally [6, 7].

The eigenstate thermalization hypothesis (ETH) explains eventual thermalization by postulating a particular structure of matrix elements of observable  $\mathcal{O}$  in the eigenbasis of a generic Hamiltonian  $\mathcal{H}$  [8–10],

$$\mathcal{O}_{mn} = O(\bar{E})\delta_{mn} + \Omega^{-1/2}(\bar{E})f(\bar{E}, \omega)r_{mn}, \quad (1)$$

where  $\omega = E_m - E_n$ ,  $\bar{E} = (E_m + E_n)/2$ , and  $\mathcal{O}_{mn} = \langle m|\mathcal{O}|n\rangle$ , with  $E_m$  and  $|m\rangle$  denoting the eigenvalues and eigenstates of  $\mathcal{H}$ . Moreover,  $\Omega(\bar{E})$  is the density of states,  $O(\bar{E})$  and  $f(\bar{E}, \omega)$  are smooth functions, and the  $r_{mn} = r_{nm}^*$  are usually assumed to be independent random Gaussian variables with zero mean and unit variance. While the general features of the ETH have been numerically confirmed for various nonintegrable models [11–20], recent works have proposed further generalizations [21–24], and scrutinized detailed aspects such as entanglement structure of highly excited eigenstates [25], or the presence of rare ETH-violating states [26].

The formulation of the ETH in Eq. (1) may essentially be regarded as an extension of the random-matrix theory (RMT) applied to observables. Numerical analyses have yielded a convincing agreement with the predictions of RMT, for instance regarding the Gaussianity of the  $r_{mn}$  [18, 27], or the ratio of variances of the diagonal and off-diagonal matrix elements [3, 16, 17, 28].

At the same time, it is clear that physical Hamiltonians and observables differ from genuinely random operators (for instance, matrix elements  $\langle m|\sigma_z|n\rangle$  of a Pauli operator must be correlated to yield the eigenvalues  $\pm 1$ ). In this context, the question whether and to what extent the  $r_{mn}$  in Eq. (1) can indeed be considered as *uncorrelated* random numbers has attracted increased attention recently [20, 29, 30]. In particular, it has been argued that correlations between matrix elements are necessary to explain the growth of the so-called out-of-time ordered correlation function (OTOC) [31–33], which is the central quantity to characterize scrambling in quantum many-body systems [34]. Using full eigenvalue spectrum of the operator submatrices as a sensitive indicator, correlations between matrix elements have been shown to persist to small energy scales, but appear to vanish at even lower  $\omega$  [20], indicating a transition to a genuine RMT behavior at sufficiently low frequencies. The lack of correlations between  $r_{mn}$  at low  $\omega$  is consistent with expected universality of the observable's dynamics at late times [35–38].

An important and less clear aspect is to connect the apparent onset of random-matrix behavior with the time scale of thermalization. Given a (one-dimensional) quantum many-body system of size  $L$ , thermalization of an observable  $\mathcal{O}$  is expected after a time  $\tau_{\text{th}} \propto L^\nu$ , where  $\nu \geq 0$  depends on  $\mathcal{O}$  as well as details of the system, e.g., presence of conservation laws [39], or disorder (see [40] and references therein). Somewhat unexpectedly, it was analytically shown in [29] that in one dimensional systems, macroscopic thermalization dynamics prevents matrix elements of  $\mathcal{O}$  from becoming truly uncorrelated above a parametrically smaller energy scale  $\Delta E_{\text{RMT}} \propto$

$1/(\tau_{\text{th}}L)$ , i.e., genuine RMT behavior can occur only at much later times of order  $T_{\text{RMT}} \propto 1/\Delta E_{\text{RMT}} \propto \tau_{\text{th}}L$ . We note that absence of correlations between matrix elements used in [29] and in this Letter to define the transition to RMT behavior is different from the so-called ‘‘Thouless time’’ [41] that controls applicability of RMT to describe energy spectrum, and is associated with the onset of the ramp in the spectral form factor [42–44].

From a numerical point of view, a major complication to study matrix elements is given by the usual restriction of full exact diagonalization (ED) to small system sizes, such that the analysis of low-frequency or, correspondingly, long-time regimes is plagued by severe finite-size effects. In this Letter, we introduce a novel numerical approach based on quantum typicality (see [45, 46] and references therein). In particular, we show that moments of operator submatrices, defined within energy windows of varying width, can be evaluated for system sizes beyond the range of ED and provide a sensitive probe for the onset or absence of the RMT behavior. For nonintegrable one-dimensional quantum spin models, our analysis shows that genuine RMT behavior is absent even for narrow energy windows corresponding to time scales around the thermalization time of the respective observable. For shorter times, the residual correlations between matrix elements are manifest in the nontrivial dynamics of suitably defined OTOCs within such energy windows.

*Setup.* We consider submatrices  $\mathcal{O}^T$  defined within energy windows of width  $2\pi/T$  [20, 28, 29],

$$\mathcal{O}_{mn}^T = \langle m|P_T\mathcal{O}P_T|n\rangle = \begin{cases} \mathcal{O}_{mn}, & |E_{m,n} - E_0| \leq \frac{\pi}{T} \\ 0, & \text{otherwise} \end{cases}, \quad (2)$$

where  $P_T = \sum_{|E_m - E_0| \leq \frac{\pi}{T}} |m\rangle\langle m|$  is a projection on eigenstates of  $\mathcal{H}$  centered around  $E_0$ . Here, parameter  $T$  controlling the size of the submatrix determines characteristic time scale (matrix elements at low  $\omega$  contribute to dynamics at long time scales). We will compare the energy scale  $1/T$ , where  $\mathcal{O}^T$  shows RMT behavior, with the energy scale  $1/\tau_{\text{th}}$  set by thermalization time, when the value of  $\mathcal{O}$  reaches its thermal equilibrium. Specific examples of  $\mathcal{H}$  and  $\mathcal{O}$  are given below.

We study the presence of correlations between matrix elements by introducing the ratio of moments  $\Lambda^T$ ,

$$\Lambda^T \equiv \frac{\mathcal{M}_2^2}{\mathcal{M}_4}, \quad \mathcal{M}_k = \frac{\text{Tr}[(\mathcal{O}_c^T)^k]}{d}, \quad (3)$$

where  $d = \text{Tr}[(P_T)] = \sum_{|E_m - E_0| \leq \frac{\pi}{T}} 1$  and  $\mathcal{O}_c^T = \mathcal{O}^T - \text{Tr}(\mathcal{O}^T)/d$ . Assuming that off-diagonal matrix elements are uncorrelated and the diagonal matrix elements satisfy ETH, one finds  $\Lambda^T \simeq 1/2$  [47], which is just the prediction of Wigner semicircle distribution. Thus,  $\Lambda^T \rightarrow 1/2$  can be regarded as an indication of RMT behavior.

*Numerical approach.* To construct  $\mathcal{O}^T$  explicitly without using ED, it is crucial to rewrite  $P_T$  as

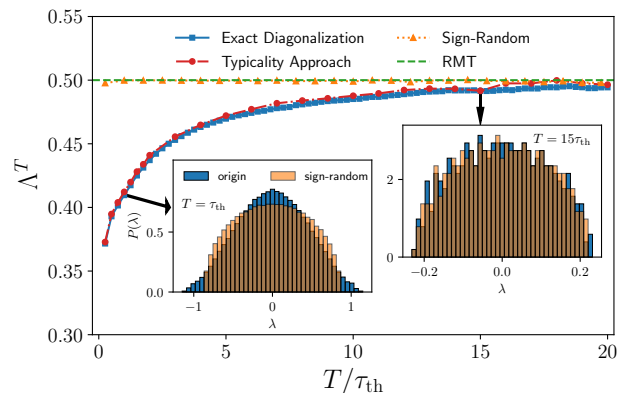


FIG. 1.  $\Lambda^T$  versus  $T/\tau_{\text{th}}$  for  $\mathcal{A}$ ,  $L = 16$  and  $q = L/2$ . Results obtained by the typicality approach [Eq. (5)], averaged over 500 states, agree convincingly with the ED data. As a comparison,  $\Lambda^T$  obtained from a sign-randomized operator [Eq. (8)] yields the RMT value  $\Lambda^T = 1/2$ . Insets show the eigenvalue distributions  $P(\lambda)$  of  $\mathcal{O}^T$  for two different energy windows.

$P_T = \frac{1}{T} \int_{-\infty}^{+\infty} \text{sinc}(t/T) \exp[-i(\mathcal{H} - E_0)t] dt$  [29], where  $\text{sinc}(t) = \sin(\pi t)/\pi t$ . In particular, by expanding the time evolution operator in terms of Chebyshev polynomials [48–50] and evaluating the integral analytically,  $P_T$  can be written as [47]

$$P_T = \sum_{k=0}^{\infty} C_k T_k\left(\frac{\mathcal{H} - b}{a}\right), \quad (4)$$

where  $T_k(x)$  are Chebyshev polynomials of the first kind,  $C_k$  are suitable coefficients (see [47]), and  $a = (E_{\text{max}} - E_{\text{min}})/2$ ,  $b = (E_{\text{max}} + E_{\text{min}})/2$ , where  $E_{\text{max}}$  and  $E_{\text{min}}$  are the largest and smallest eigenvalues of  $\mathcal{H}$ . Exploiting quantum typicality [45, 46] (see also [47] for details) one can then calculate the second and the fourth central moments of  $\mathcal{O}^T$  as

$$\mathcal{M}_2 \approx \frac{\langle \psi_{POP} | \psi_{POP} \rangle}{\langle \psi_P | \psi_P \rangle}, \quad \mathcal{M}_4 \approx \frac{\langle \psi_{(POP)^2} | \psi_{(POP)^2} \rangle}{\langle \psi_P | \psi_P \rangle}, \quad (5)$$

where  $|\psi_P\rangle = P_T|\psi\rangle$ ,  $|\psi_{POP}\rangle = P_T\mathcal{O}_c^T P_T|\psi\rangle$ ,  $|\psi_{(POP)^2}\rangle = (P_T\mathcal{O}_c^T P_T)^2|\psi\rangle$ , and  $\mathcal{O}_c^T = \mathcal{O}^T - \langle \psi_P | \mathcal{O}^T | \psi_P \rangle / \langle \psi_P | \psi_P \rangle$ . Here,  $|\psi\rangle$  is a pure state drawn at random from the unitarily invariant Haar measure [51], i.e., in practice  $|\psi\rangle$  is constructed in the computational basis with Gaussian distributed coefficients. The approximation of  $\mathcal{M}_k$  in Eq. (5) becomes very accurate for energy windows with sufficiently many eigenstates. For smaller windows with fewer eigenstates, the accuracy can be improved by averaging over multiple realizations of  $|\psi\rangle$ . The most demanding step of our numerical approach is to calculate  $P_T|\psi\rangle$ , i.e., to restrict the random state to the energy window specified by  $P_T$ ,  $P_T|\psi\rangle = \sum_{k=0}^M C_k T_k\left(\frac{\mathcal{H} - b}{a}\right)|\psi\rangle$ , where Eq. (4) is approximated by the summation up to  $k = M$ , where  $M$  has to be chosen large enough to yield accurate results [52].

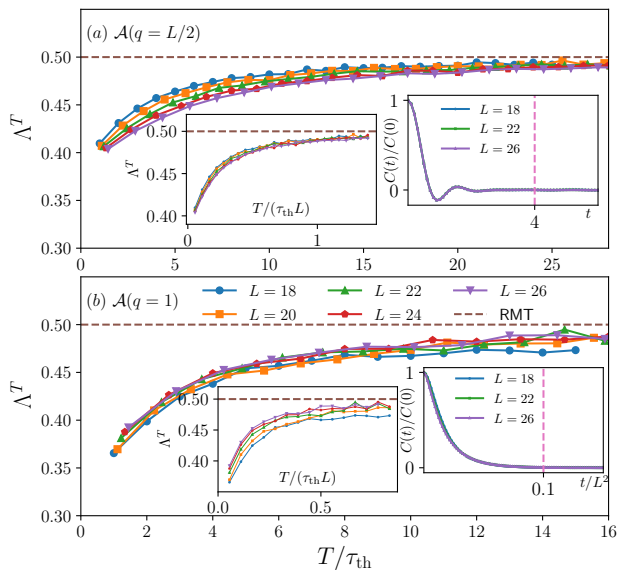


FIG. 2.  $\Lambda^T$  versus  $T/\tau_{th}$  for the density-wave operator  $\mathcal{A}$  with (a)  $q = L/2$  and (b)  $q = 1$ . Data is obtained using typicality approach, averaged over  $500 \cdot (\frac{16}{L})^2$  states, for up to  $L = 26$ . The dashed horizontal line indicates the RMT value  $\Lambda^T = 0.5$ . The two insets show  $\Lambda^T$  versus  $T/(\tau_{th}L)$  and the autocorrelation function  $C(t) = \text{Tr}[\mathcal{A}(t)\mathcal{A}]/2^L$ , normalized by its initial value, where the dashed vertical line indicates the thermalization time  $\tau_{th}$ . Good quality of collapse of  $C(t)$  and  $C(t/L^2)$  correspondingly for different  $L$  confirms  $L$ -independence of  $\tau_{th}$  for  $q = L/2$  and diffusive behavior  $\tau_{th} \propto L^2$  for  $q = 1$ .

Crucially, this step can be achieved by means of sparse-matrix techniques such that  $\mathcal{M}_k$  and therefore  $\Lambda^T$  can be obtained for Hilbert-space dimensions far beyond the range of the ED. To conclude, we note that other approaches exist to construct states within a specified energy window [53], e.g., using a Gaussian filter [54, 55].

*Numerical analysis.* We consider one-dimensional mixed-field Ising model,  $\mathcal{H} = \sum_{\ell=1}^L \mathcal{H}^\ell$ ,

$$\mathcal{H}^\ell = J\sigma_z^\ell \sigma_z^{\ell+1} + \frac{h_x}{2}(\sigma_x^\ell + \sigma_x^{\ell+1}) + \frac{h_z}{2}(\sigma_z^\ell + \sigma_z^{\ell+1}), \quad (6)$$

where  $\sigma_{x,z}^\ell$  are Pauli operators at lattice site  $\ell$ ,  $L$  is the length of the chain with periodic boundaries, and  $J = h_x = 1.0$  and  $h_z = 0.5$  in the following. Moreover, we add two defect terms  $h_2\sigma_z^2$  and  $h_5\sigma_z^5$  with  $h_2 = 0.165$  and  $h_5 = -0.24$  to lift translational and reflection symmetries. We note that  $\mathcal{H}$  is nonintegrable, fulfills the ETH for these parameters [47], and exhibits diffusive energy transport [56]. We consider energy windows centered around  $E_0 = 0$ , corresponding to infinite temperature. We study  $\Lambda^T$  for two kinds of operators,

$$\mathcal{A} = \frac{1}{\sqrt{L}} \sum_{\ell=1}^L \cos\left(\frac{2\pi}{L}q\ell\right) \mathcal{H}^\ell, \quad \mathcal{B} = \frac{1}{\sqrt{L}} \sum_{\ell=1}^L \sigma_x^\ell, \quad (7)$$

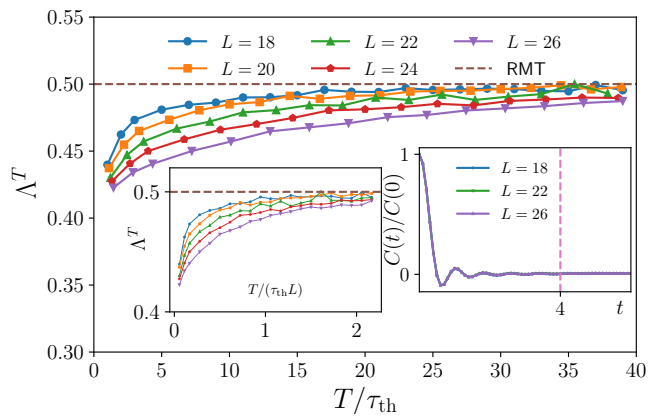


FIG. 3. Analogous data as in Fig. 2, but now for  $\mathcal{B}$ .

where  $\mathcal{B}$  exhibits no transport behavior and decays quickly. In contrast, dynamics of the density-wave operator  $\mathcal{A}$  depends on  $q$ , with a quick  $L$ -independent decay for  $q = L/2$  and a slow hydrodynamic (diffusive) relaxation in the limit of small  $q$  [39]. For our numerical analysis, operators with short,  $L$ -independent  $\tau_{th}$ , are beneficial as this allows us numerically to reach regimes  $T/\tau_{th} \gg 1$ , which in contrast becomes very costly if  $\tau_{th} \propto L^2$  scales diffusively with the system size.

A first glance of how  $\Lambda^T$  behaves upon varying the width of the energy window is given in Fig. 1, where we consider  $\mathcal{A}$  for a small system with  $L = 16$  amenable to ED. ED values of  $\Lambda^T$  show convincing agreement with those obtained using typicality approach for a wide range of  $T$ . Analyzing  $\Lambda^T$  behavior, we see that it deviates from the RMT value for small  $T$  (i.e., large energy windows), but approaches it for larger  $T$ . As shown in the insets of Fig. 1, the full eigenvalue distribution  $P(\lambda)$  of  $\mathcal{A}^T$  is approximately Gaussian for small  $T$  ( $\Lambda^T = 1/3$  for strictly Gaussian distributions), while it takes an approximately semicircle shape for larger  $T$ , indicating a transition to the RMT behavior [20]. It is further helpful to compare the data for a given  $\mathcal{O}^T$  with a sign-randomized version of the operator, [20, 57, 58],

$$\tilde{\mathcal{O}}_{mn}^T = \begin{cases} \mathcal{O}_{mn}^T, & 50\% \text{ probability} \\ (-1)\mathcal{O}_{mn}^T, & 50\% \text{ probability} \end{cases}, \quad (8)$$

which exhibits no correlations between matrix elements. As shown in Fig. 1,  $\tilde{\mathcal{A}}^T$  indeed yields  $\Lambda^T \approx 0.5$  with semicircular  $P(\lambda)$  for all  $T$  considered here, which further confirms that  $\Lambda^T \rightarrow 0.5$  is a good indicator to probe the onset of RMT behavior.

In the following, we study dependence of  $\Lambda^T$  on  $T$  for larger systems up to  $L = 26$  using typicality approach introduced above. First we consider operator  $\mathcal{O} = \mathcal{A}$  with  $q = L/2$  for which the autocorrelation function,

$$C(t) = \text{Tr}[\mathcal{O}(t)\mathcal{O}]/2^L, \quad (9)$$

decays quickly towards an approximately constant value on a  $L$ -independent time scale, which we identify as the thermalization time  $\tau_{\text{th}}$ , see inset in Fig. 2 (a). Note that  $C(t)$  is also obtained with help of typicality approach [45, 46, 59]. Inspecting the value of  $\Lambda^T$  at the energy scale which corresponds to thermalization,  $T \approx \tau_{\text{th}}$ , we find it is far from the RMT value but tends to approach it at larger values of  $T$ . The same behavior of  $\Lambda^T$  is also demonstrated by the second operator  $\mathcal{O} = \mathcal{B}$ , see Fig. 3. Specifically, it also has  $L$ -independent thermalization time scale  $\tau_{\text{th}}$  (see inset in Fig. 3), and for  $T \approx \tau_{\text{th}}$  the value of  $\Lambda^T$  is far from its asymptotic value 0.5.

Next we consider density-wave operator  $\mathcal{A}$  with the longest wavelength,  $q = 1$ . This is a diffusive operator, and corresponding two-point function  $C(t)$  decays exponentially, with the relevant timescale  $\tau_{\text{th}} \propto L^2$ . This scaling is confirmed by the collapse of  $C(t/L^2)$  for different  $L$  as shown the inset of Fig. 2 (b). As before, we find that the value of  $\Lambda^T$  is far from the RMT prediction for  $T \approx \tau_{\text{th}}$ , while it tends to approach it for larger  $T$ . Thus in all cases shown in Figs. 2 and 3, we conclude that submatrices  $\mathcal{O}^T$  exhibit significant deviations from the RMT behavior for energy scale defined by inverse thermalization time  $\tau_{\text{th}}$ , consistent with [29]. The onset of strict RMT behavior may occur only at much longer times  $T_{\text{RMT}} \gg \tau_{\text{th}}$ . This is the main result of this Letter.

It would be a natural step to quantify  $T_{\text{RMT}}/\tau_{\text{th}}$  for different operators, and in particular its dependence on the system size  $L$ . In practice this requires extending numerical analysis to much larger values of  $T$ , for which  $\Lambda^T \approx 0.5$ , which is a challenging task. Here, we particularly focus on the case of  $\mathcal{A}$  with  $q = L/2$ . By plotting  $\Lambda^T$  versus  $T/(\tau_{\text{th}}L)$ , see inset in Fig. 2 (a), we observe a good numerical collapse extending through all values of  $T$ . This tentatively suggest  $T_{\text{RMT}} \propto \tau_{\text{th}}L$  at least for this operator. In [47], we provide additional data for another model, nonintegrable XXZ chain with next-nearest neighbor interactions, and an observable exhibiting diffusive spin transport. In that case the data is also consistent with the scaling  $T_{\text{RMT}} \propto \tau_{\text{th}}L$ . We note that for other operators  $\Lambda^T$ , plotted as a function of  $T/(\tau_{\text{th}}L)$  may not show collapse for small and moderate  $T$  [cf. insets in Figs. 2 (b) and 3]. This is not directly contradicting  $T_{\text{RMT}} \propto \tau_{\text{th}}L$  as only collapse in the region of large  $T \approx T_{\text{RMT}}$  would be necessary to confirm that scaling.

*Dynamics of OTOCs.* Presence of correlations between matrix elements of  $\mathcal{O}$  also manifests itself in the dynamical properties [30]. In particular, here we consider out-of-time-ordered correlation function suitably defined within the energy window  $|E_m - E_0| \leq \frac{\pi}{T}$ ,

$$F_T(t) = \text{Tr}[\mathcal{O}_c^T(t)\mathcal{O}_c^T(t)\mathcal{O}_c^T(t)\mathcal{O}_c^T(t)]. \quad (10)$$

Assuming that off-diagonal matrix elements of  $\mathcal{O}_c^T$  are uncorrelated and that diagonal elements satisfy ETH

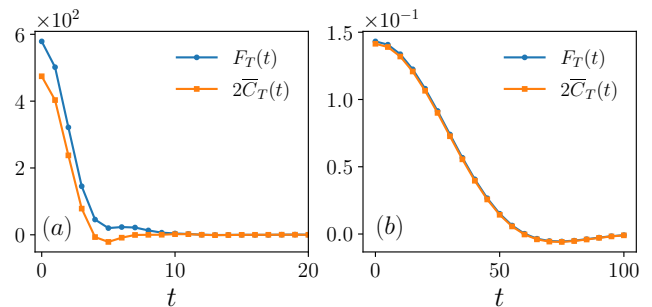


FIG. 4.  $F_T(t)$  [Eq. (10)] and  $2\overline{C}_T(t)$  [Eq. (12)] for  $\mathcal{A}$  with  $q = L/2$  and  $L = 16$  for (a)  $T = \tau_{\text{th}}$  and (b)  $T = 15\tau_{\text{th}}$ .

[47],  $F_T(t)$  should reduce to

$$F_T(t) \simeq 2\overline{C}_T(t), \quad (11)$$

where  $\overline{C}_T(t)$  is the following eigenstate-averaged two-point function,

$$\overline{C}_T(t) \equiv \sum_{m=1}^d \Re \langle m | \mathcal{O}_c^T(t) \mathcal{O}_c^T | m \rangle^2. \quad (12)$$

In Fig. 4, we study  $F_T(t)$  and  $\overline{C}_T(t)$  for the density-wave operator  $\mathcal{A}$  with  $q = L/2$ , cf. Fig. 2 (a). We consider  $L = 16$  and two different widths of the energy window,  $T = \tau_{\text{th}}$ , Fig. 4 (a), and  $T = 15\tau_{\text{th}}$ , Fig. 4 (b). In the former case, we find  $F_T(t) \neq 2\overline{C}_T(t)$ , which is consistent with our earlier observation that  $\Lambda^T \neq 0.5$  for  $T = \tau_{\text{th}}$  and supports our conclusion that higher-order correlations exist between the matrix elements of  $\mathcal{O}^T$ . In contrast, in the latter case,  $F_T(t) \approx 2\overline{C}_T(t)$ , consistent with  $\Lambda^T \rightarrow 0.5$  and signaling that correlations between matrix elements vanish and genuine RMT behavior emerges for such narrow energy windows.

*Conclusion & Outlook.* We have studied presence of correlations between matrix elements of observables written in the energy eigenbasis of chaotic quantum many-body systems. We introduced a novel numerical method to evaluate higher moments of operator submatrices for system sizes beyond those accessible by ED. As a main result, we have shown that even for narrow energy windows, corresponding to time scales of the order of thermalization time for the given observable, genuine RMT behavior is absent. Consistent with the results of [20, 29], our findings suggest that even though usual indicators of the ETH might be completely fulfilled [47], ETH has to be refined to properly describe all dynamical aspects of thermalization. Specifically, in addition to the usual thermalization or Thouless time controlling RMT behavior of energy levels, there exists another relevant scale  $T_{\text{RMT}}$ , which corresponds to the onset of genuine RMT behavior in the matrix elements of observables. We find that only at late times,  $T_{\text{RMT}} \gg \tau_{\text{th}}$  dynamics may be fully consistent with the RMT description. We have



also demonstrated this fact by studying suitably defined OTOCs, which visualized the presence of higher-order correlations between matrix elements well beyond thermalization time of the corresponding two-point function.

It would be a natural next step to systematically study  $L$  dependence of  $T_{\text{RMT}}/\tau_{\text{th}}$  for various operators and clarify the role of conservation laws giving rise to hydrodynamic behavior at late times. Thus, it would be interesting to consider time-dependent Floquet models without energy conservation. Another direction is to study the onset of RMT behavior in disordered systems which may exhibit subdiffusive transport or localization depending on the strength of the disorder [60].

*Acknowledgements.* This work has been funded by the Deutsche Forschungsgemeinschaft (DFG), Grants No. 397107022 (GE 1657/3-2), No. 397067869 (STE 2243/3-2), and No. 355031190, within the DFG Research Unit FOR 2692. J. R. has been funded by the European Research Council (ERC) under the European Union's Horizon 2020 research and innovation programme (Grant agreement No. 853368). A. D. acknowledges support of the Russian Science Foundation (Project No. 17-12-01587).

---

\* [jiaozi.wang@uos.de](mailto:jiaozi.wang@uos.de)

† [jgemmer@uos.de](mailto:jgemmer@uos.de)

- [1] A. Polkovnikov, K. Sengupta, A. Silva, and M. Vengalattore, *Rev. Mod. Phys.* **83**, 863 (2011).
- [2] C. Gogolin and J. Eisert, *Rep. Prog. Phys.* **79**, 056001 (2016).
- [3] L. D'Alessio, Y. Kafri, A. Polkovnikov, and M. Rigol, *Adv. Phys.* **65**, 239 (2016).
- [4] F. Borgonovi, F. M. Izrailev, L. F. Santos, and V. G. Zelevinsky, *Phys. Rep.* **626**, 1 (2016).
- [5] T. Mori, T. N. Ikeda, E. Kaminshi, and M. Ueda, *J. Phys. B: At. Mol. Opt. Phys.* **51**, 112001 (2018).
- [6] S. Trotzky, Y.-A. Chen, A. Flesch, I. P. McCulloch, U. Schollwöck, J. Eisert, and I. Bloch, *Nat. Phys.* **8**, 325 (2012).
- [7] A. M. Kaufmann, M. E. Tai, A. Lukin, M. Rispoli, R. Schittko, P. M. Preiss, and M. Greiner, *Science* **353**, 794 (2016).
- [8] J. M. Deutsch, *Phys. Rev. A* **43**, 2046 (1991).
- [9] M. Srednicki, *Phys. Rev. E* **50**, 888 (1994).
- [10] M. Rigol, V. Dunjko, and M. Olshanii, *Nature* **452**, 854 (2008).
- [11] R. Steinigeweg, J. Herbrych, and P. Prelovšek, *Phys. Rev. E* **87**, 012118 (2013).
- [12] W. Beugeling, R. Moessner, and M. Haque, *Phys. Rev. E* **89**, 042112 (2014).
- [13] H. Kim, T. N. Ikeda, D. A. Huse, *Phys. Rev. E* **90**, 052105 (2014).
- [14] E. J. Torres-Herrera and L. F. Santos, *Phys. Rev. E* **89**, 062110 (2014).
- [15] R. Mondaini, K. R. Fratus, M. Srednicki, and M. Rigol, *Phys. Rev. E* **93**, 032104 (2016).
- [16] R. Mondaini and M. Rigol, *Phys. Rev. E* **96**, 012157 (2017).
- [17] D. Jansen, J. Stolpp, L. Vidmar, and F. Heidrich-Meisner, *Phys. Rev. B* **99**, 155130 (2019).
- [18] T. LeBlond, K. Mallayya, L. Vidmar, and M. Rigol, *Phys. Rev. E* **100**, 062134 (2019).
- [19] M. Brenes, T. LeBlond, J. Goold, and M. Rigol, *Phys. Rev. Lett.* **125**, 070605 (2020).
- [20] J. Richter, A. Dymarsky, R. Steinigeweg, and J. Gemmer, *Phys. Rev. E* **102**, 042127 (2020).
- [21] J. Richter, J. Gemmer, and R. Steinigeweg, *Phys. Rev. E* **99**, 050104(R) (2019).
- [22] A. Dymarsky and K. Pavlenko, *Phys. Rev. Lett.* **123**, 111602 (2019).
- [23] K. Kaneko, E. Iyoda, and T. Sagawa, *Phys. Rev. A* **101**, 042126 (2020).
- [24] M. Mierzejewski and L. Vidmar, *Phys. Rev. Lett.* **124**, 040603 (2020).
- [25] M. Brenes, S. Pappalardi, J. Goold, and A. Silva, *Phys. Rev. Lett.* **124**, 040605 (2020).
- [26] M. Serbyn, D. A. Abanin, and Z. Papić, *Nat. Phys.* **17**, 675 (2021).
- [27] D. J. Luitz, I. M. Khaymovich, and Y. Bar Lev, *SciPost Phys. Core* **2**, 006 (2020).
- [28] A. Dymarsky and H. Liu, *Phys. Rev. E* **99**, no.1, 010102 (2019).
- [29] A. Dymarsky, arXiv:1804.08626.
- [30] M. Brenes, S. Pappalardi, M. T. Mitchison, J. Goold, and A. Silva, arXiv:2103.01161.
- [31] L. Foini and J. Kurchan, *Phys. Rev. E* **99**, 042139 (2019).
- [32] A. Chan, A. De Luca, and J. T. Chalker, *Phys. Rev. Lett.* **122**, 220601 (2019).
- [33] C. Murthy and M. Srednicki, *Phys. Rev. Lett.* **123**, 230606 (2019).
- [34] B. Swingle, G. Bentsen, M. Schleier-Smith, and P. Hayden, *Phys. Rev. A* **94**, 040302(R) (2016).
- [35] J. Cotler, N. Hunter-Jones, J. Liu, and Beni Yoshida, *JHEP* **2017**, 48 (2017).
- [36] J. Cotler and N. Hunter-Jones, arXiv:1911.02026 (2019).
- [37] S. Moudgalya, T. Devakul, C. W. von Keyserlingk, and S. L. Sondhi, *Phys. Rev. B* **99**, 094312 (2019).
- [38] M. Schiulaz, E. J. Torres-Herrera, and L. F. Santos, *Phys. Rev. B* **99**, 174313 (2019).
- [39] B. Bertini, F. Heidrich-Meisner, C. Karrasch, T. Prosen, R. Steinigeweg, and M. Žnidarič, *Rev. Mod. Phys.* **93**, 025003 (2021).
- [40] D. A. Abanin, E. Altman, I. Bloch, and M. Serbyn, *Rev. Mod. Phys.* **91**, 021001 (2019).
- [41] J. T. Edwards and D. J. Thouless, *J. Phys. C* **5**, 807 (1972).
- [42] J. Šuntajs, J. Bonča, T. Prosen, L. Vidmar, *Phys. Rev. E* **102**, 062144 (2020).
- [43] P. Kos, B. Bertini, and T. Prosen, *Phys. Rev. Lett.* **126**, 190601 (2021).
- [44] S. Moudgalya, A. Prem, D. A. Huse, and A. Chan, *Phys. Rev. Research* **3**, 023176 (2021).
- [45] F. Jin, D. Willsch, M. Willsch, H. Lagemann, K. Michielsen, and H. De Raedt, *J. Phys. Soc. Jpn.* **90**, 012001 (2021).
- [46] T. Heitmann, J. Richter, D. Schubert, and R. Steinigeweg, *Z. Naturforsch. A* **75**, 421 (2020).
- [47] See supplemental material for details on the value of  $\Lambda^T$  for uncorrelated matrix elements, our numerical typicality approach, ETH indicators for  $\mathcal{H}$ , additional results for other models and observables, and a derivation of Eq. (11).

- [48] H. Tal-Ezer and R. Kosloff, J. Chem. Phys. **81**, 3967 (1984).
- [49] V. V. Dobrovitski and H. De Raedt, Phys. Rev. E **67**, 056702 (2003).
- [50] A. Weiße, G. Wellein, A. Alvermann, and H. Fehske, Rev. Mod. Phys. **78**, 275 (2006).
- [51] C. Bartsch and J. Gemmer, Phys. Rev. Lett. **102**, 110403 (2009).
- [52] In our simulations, we choose  $M = 6aT$ , which yields relatively accurate values for  $\Lambda^T$ , but is still low enough such that numerical costs remain reasonable.
- [53] Y. Yamaji, T. Suzuki, and M. Kawamura, arXiv:1802.02854.
- [54] S. Garnerone and T. R. de Oliveira, Phys. Rev. B **87**, 214426 (2013).
- [55] R. Steinigeweg, A. Khodja, H. Niemeyer, C. Gogolin, and J. Gemmer, Phys. Rev. Lett. **112**, 130403 (2014).
- [56] H. Kim and D. A. Huse, Phys. Rev. Lett. **111**, 127205 (2013).
- [57] D. Cohen and T. Kottos, Phys. Rev. E **63**, 036203 (2001).
- [58] T. Kottos and D. Cohen, Phys. Rev. E **64**, 065202(R) (2001).
- [59] T. Elsayed and B. Fine, Phys. Rev. Lett. **110**, 070404 (2013).
- [60] S. Gopalakrishnan, S. A. Parameswaran, Physics Reports **862**, 1 (2020).

## Supplemental material

### EVALUATION OF $\Lambda^T$ FOR MATRICES WITH UNCORRELATED ELEMENTS

In order to evaluate the value of  $\Lambda^T$ , let's write the fourth moment  $\mathcal{M}_4$  [Eq.(3) in the main text] in the energy basis,

$$\mathcal{M}_4 = \frac{1}{d} \sum_{m n k l} (\mathcal{O}_c^T)_{mn} (\mathcal{O}_c^T)_{nk} (\mathcal{O}_c^T)_{kl} (\mathcal{O}_c^T)_{lm}. \quad (\text{S1})$$

$|E_m - E_0| \leq \frac{\pi}{T}$ . Recalling the definition of  $\mathcal{O}_c^T$

$$\mathcal{O}_c^T = \mathcal{O}^T - \frac{\text{Tr}(\mathcal{O}^T)}{d}, \quad (\text{S2})$$

one has  $(\mathcal{O}_c^T)_{mm} \simeq 0$  within the energy window  $|E_m - E_0| \leq \frac{\pi}{T}$  for sufficiently large  $T$  in case that  $\mathcal{O}^T$  satisfies ETH. Assuming that the elements  $(\mathcal{O}_c^T)_{mn}$  are uncorrelated, only the ‘‘square’’ terms in the summation of Eq. (S1) are non-negligible. Thus, one gets (we omit the subscript  $c$  in  $\mathcal{O}_c^T$  for simplicity in the following),

$$\begin{aligned} \mathcal{M}_4 &= \frac{1}{d} \sum_{mnl} |\mathcal{O}_{mn}^T|^2 |\mathcal{O}_{lm}^T|^2 + \frac{1}{d} \sum_{mnk} |\mathcal{O}_{mn}^T|^2 |\mathcal{O}_{kn}^T|^2 \\ &= \frac{2}{d} \sum_m \left( \sum_n |\mathcal{O}_{mn}^T|^2 \right)^2 = \frac{2}{d} \sum_m (\langle m | (\mathcal{O}^T)^2 | m \rangle)^2. \end{aligned} \quad (\text{S3})$$

With the further assumption that the diagonal elements of  $(\mathcal{O}_c^T)^2$  are constant within  $|E_m - E_0| \leq \frac{\pi}{T}$ , one has

$$\begin{aligned} \langle m | (\mathcal{O}^T)^2 | m \rangle &\simeq \frac{1}{d} \sum_{m'} \langle m' | (\mathcal{O}^T)^2 | m' \rangle \\ &= \begin{cases} \mathcal{M}_2 & |E_m - E_0| \leq \frac{\pi}{T} \\ 0 & \text{otherwise.} \end{cases} \end{aligned} \quad (\text{S4})$$

Substituting Eq. (S4) into Eq. (S3) yields,

$$\mathcal{M}_4 \simeq \frac{2}{d} \sum_m \mathcal{M}_2^2 = 2\mathcal{M}_2^2, \quad (\text{S5})$$

and

$$\Lambda^T \simeq 0.5, \quad (\text{S6})$$

which is just the prediction of the Wigner semicircle spectrum.

### REDUCTION OF $OTO$ C TO TWO-POINT CORRELATION FUNCTIONS

In the energy eigenbasis, the out-of-time-ordered correlator  $F_T(t)$  [Eq. (10) in the main text] can be written as,

$$F_T(t) = \sum_{m n k l} \mathcal{O}_{mn}^T \mathcal{O}_{nk}^T \mathcal{O}_{kl}^T \mathcal{O}_{lm}^T e^{-i(E_n - E_m + E_l - E_k)t}. \quad (\text{S7})$$

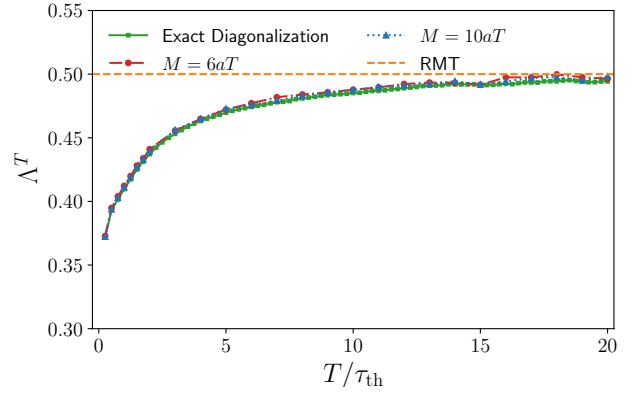


FIG. S1.  $\Lambda^T$  versus  $T/\tau_{th}$  for  $\mathcal{A}$  and system size  $L = 16$  in Ising model. Results are obtained by the typicality approach, averaged over 500 states, for two different value of  $M = 6aT$  (red) and  $M = 10aT$  (orange)

Assuming that matrix elements  $\mathcal{O}_{mn}^T$  are uncorrelated, and that the diagonal elements  $\mathcal{O}_{mm}^T \approx 0$  vanish within  $|E_m - E_0| \leq \frac{\pi}{T}$ , using arguments similar as in the last section that (see also [S9]), one finds that

$$\begin{aligned} F_T(t) &\simeq \sum_m \sum_n |\mathcal{O}_{mn}^T|^2 e^{-i(E_n - E_m)t} \sum_l |\mathcal{O}_{ml}^T|^2 e^{-i(E_l - E_m)t} \\ &\quad + \sum_n \sum_m |\mathcal{O}_{nm}^T|^2 e^{-i(E_n - E_m)t} \sum_l |\mathcal{O}_{nk}^T|^2 e^{-i(E_n - E_k)t} \\ &= \sum_m \left( \sum_n |\mathcal{O}_{mn}^T|^2 e^{-i(E_n - E_m)t} \right)^2 + c.c. \\ &= 2 \sum_m \Re(\langle m | \mathcal{O}^T(t) \mathcal{O}^T | m \rangle^2) \\ &= 2\overline{C}_T(t). \end{aligned} \quad (\text{S8})$$

### DETAILS ON THE NUMERICAL TYPICALITY APPROACH

In this section, we discuss some details on our numerical typicality approach. To begin with, we show the detailed derivation of Eqs. (4) to (6) in the main text.

To this end, it is useful to rewrite  $\exp(-i(\mathcal{H} - E_0)t)$  as

$$\exp(-i(\mathcal{H} - E_0)t) = \exp(-i(b - E_0)t) \exp(-iat\mathcal{H}), \quad (\text{S9})$$

where the second term can be expanded in terms of Chebyshev Polynomial of the first kind [denoted by  $T_k(x)$ ],

$$\exp(-iat\mathcal{H}) = J_0(at) + 2 \sum_{k=1}^{\infty} (-i)^k J_k(at) T_k\left(\frac{\mathcal{H} - b}{a}\right), \quad (\text{S10})$$

where  $a = (E_{\max} - E_{\min})/2$ ,  $b = (E_{\max} + E_{\min})/2$ . Substituting Eqs.(S9) and (S10) into the definition of  $P_T$  in

FIG. S2. Diagonal matrix elements of operator (a)  $A(q = L=2)$  (b)  $A(q = 1)$  (c)  $B$  in the eigenbasis of  $H$ , for system sizes  $L = 12; 14; 16$  in Ising model.

the main text, one has

$$\begin{aligned}
 P_T &= \frac{1}{T} \int_{-T}^{T+1} \text{sinc}\left(\frac{t}{T}\right) \exp(-i(H - E_0)t) dt \quad (\text{S11}) \\
 &= \frac{1}{T} \int_{-1}^{T+1} \text{sinc}\left(\frac{t}{T}\right) \exp(-i(b - E_0)t) \\
 &\quad J_0(at) T_0\left(\frac{H - b}{a}\right) + 2 \sum_{k=1}^{\infty} (-i)^k J_k(at) T_k\left(\frac{H - b}{a}\right) dt : \quad (\text{S12})
 \end{aligned}$$

After calculating the integral in Eq.(S12) analytically, one gets

$$P_T = \sum_{k=0}^{\infty} C_k T_k\left(\frac{H - b}{a}\right); \quad (\text{S13})$$

where

$$C_0 = \frac{1}{a} \frac{\arcsin\left(\frac{\bar{T} + b - E_0}{a}\right)}{\arcsin\left(\frac{\bar{T} + b - E_0}{a}\right)}; \quad (\text{S14})$$

and

$$\begin{aligned}
 C_k(k > 1) &= \frac{2(-1)^{k+1}}{k} \frac{\sin\left(k \arccos\left(\frac{\bar{T} + b - E_0}{a}\right)\right)}{\sin\left(k \arccos\left(\frac{\bar{T} + b - E_0}{a}\right)\right)}; \quad (\text{S15})
 \end{aligned}$$

under the condition

$$a + b + \bar{T} - E_0 > a + b - \bar{T}; \quad (\text{S16})$$

which is always fulfilled in our simulations as we only consider the middle region of the spectrum.

FIG. S3. ( ! ) for matrix elements of operator (a)  $A(q = L=2)$  (b)  $A(q = 1)$  (c)  $B$  in the energy window  $E \in [0.5; 0.5]$  and system sizes  $L = 12; 14; 16$  in Ising model.

In order to study Eq. (S13) numerically, we consider only a finite number of terms in the summation,

$$P_T = \sum_{k=0}^M C_k T_k\left(\frac{H - b}{a}\right); \quad (\text{S17})$$

In our numerical simulations, we choose  $M = 6aT$ , which yields relatively accurate values for  $P_T$ , but is still low enough such that numerical costs remain reasonable. In Fig. S1, we compare the results of two different choices of  $M$ ,  $M = 6aT$  and  $M = 10aT$ , where one can see that the results are very close and both agree convincingly with the accurate result obtained by exact diagonalization.

In our numerical approach, we calculate the moments  $M_k$  by making use of quantum typicality [S2, S3]. The variance of the statistical error within this approach scales as  $1/d_e$ , where  $d_e$  is the effective dimension of the Hilbert space on which the operator is defined. For a fixed energy window, our approximation becomes more accurate for larger system sizes  $L$ , as  $d_e$  usually scales exponentially with  $L$ . Even for moderate system sizes, one can improve the accuracy by averaging over  $N$  different realizations of random states, which can reduce the variance by a factor  $N$ . In our numerical simulations,  $N$  is adjusted as a function of system  $L$ ,  $N \propto \frac{1}{2^L}$ , which yields similar accuracy for different system sizes.

## USUAL INDICATORS OF THE ETH

### Diagonal matrix elements

As a first step, we study the diagonal part of the ETH. To this end, Fig. S2 shows the matrix elements  $\langle m|A|m \rangle$  and  $\langle m|B|m \rangle$ , for different system sizes  $L = 12; 14; 16$  in



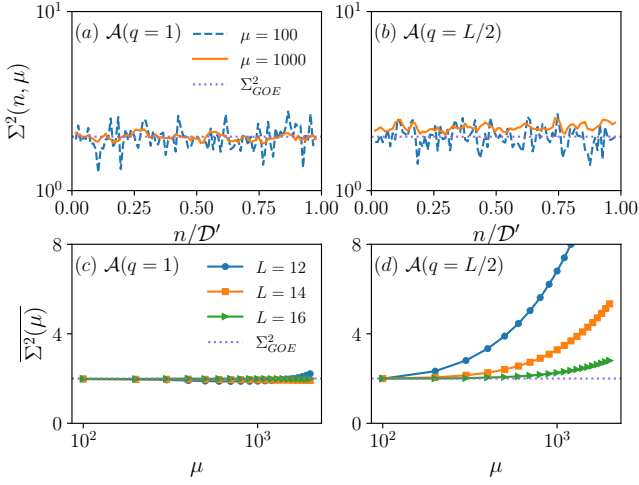


FIG. S4. [(a),(b)] Ratio  $\Sigma^2(n, \mu)$  between the variances of diagonal and off-diagonal matrix elements for two different square sizes  $\mu = 100, 1000$  and all embeddings  $n \in [1 + \mu/2, \mathcal{D} - \mu/2]$  for operator  $\mathcal{A}$  in Ising model. The data are obtained for system size  $L = 16$  and the dashed line indicates the RMT prediction  $\Sigma_{GOE}^2 = 2$ . [(c),(d)] Average value  $\overline{\Sigma^2(\mu)}$  versus  $\mu$  for system sizes  $L = 12, 14, 16$ . Panels (a) and (c) show data for  $q = L/2$ , while (b) and (d) show data for  $q = 1$ .

the Ising model. For energy densities in the center of the spectrum, we find that the “cloud” of matrix elements becomes narrower with increasing  $L$ , which is in good accord with the ETH prediction that the  $\mathcal{O}_{mm}$  should form a “smooth” function of energy in the thermodynamic limit  $L \rightarrow 0$ , and that the fluctuation of  $\mathcal{O}_{mm}$  decays exponentially with  $L$ .

### Off-diagonal matrix elements

Then we turn to analyze the properties of the off-diagonal matrix elements  $\mathcal{O}_{mn}$ , where we focus on the eigenstates with mean energy  $\frac{E_m + E_n}{2} \in [-0.5, 0.5]$ . Assuming the  $\mathcal{O}_{mn}$  have zero mean, i.e.  $\overline{\mathcal{O}_{mn}} = 0$  (which holds with a very high accuracy), we study a frequency-dependent ratio  $\Gamma(\omega)$ , recently introduced in Ref. [S5],

$$\Gamma(\omega) = \frac{\overline{|\mathcal{O}_{mn}|^2}(\omega)}{|\overline{\mathcal{O}_{mn}}(\omega)|^2}. \quad (\text{S18})$$

where

$$\overline{|\mathcal{O}_{mn}|^2}(\omega) = \frac{1}{N_\omega} \sum_{\substack{m,n \\ |E_m - E_n| \approx \omega}} |\mathcal{O}_{mn}|^2, \quad (\text{S19})$$

$$\overline{|\mathcal{O}_{mn}|}(\omega) = \frac{1}{N_\omega} \sum_{\substack{m,n \\ |E_m - E_n| \approx \omega}} |\mathcal{O}_{mn}|. \quad (\text{S20})$$

Here the sum runs over all  $N_\omega$  matrix elements with  $|E_m - E_n| \in [\omega - \Delta\omega/2, \omega + \Delta\omega/2]$ , where we choose

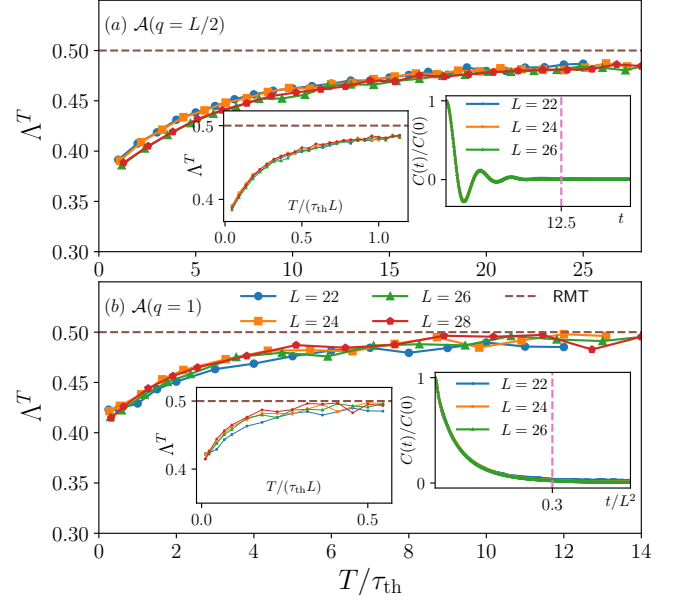


FIG. S5.  $\Lambda^T$  versus  $T/\tau_{th}$  for the spin density-wave operator  $\mathcal{A}_s$  (S24) in XXZ model (described by  $\mathcal{H}_2$ ) with (a)  $q = L/2$  and (b)  $q = 1$ . Data is obtained using typicality approach, averaged over  $500 \times (\frac{18}{L})^2$  states, for up to  $L = 28$ . The dashed horizontal line indicates the RMT value  $\Lambda^T = 0.5$ . The two insets show  $\Lambda^T$  versus  $T/(\tau_{th}L)$  and the autocorrelation function  $C(t) = \text{Tr}[\mathcal{A}_s(t)\mathcal{A}_s]/2^L$ , normalized by its initial value, where the dashed vertical line indicates the thermalization time  $\tau_{th}$ . Good quality of collapse of  $C(t)$  and  $C(t/L^2)$  correspondingly for different  $L$  confirms  $L$ -independence of  $\tau_{th}$  for  $q = L/2$  and diffusive behavior  $\tau_{th} \propto L^2$  for  $q = 1$ .

$\Delta\omega = 0.05$  in our numerical simulation. In Fig. S3 we find that  $\Gamma(\omega)$  is close to the Gaussian value  $\pi/2$  for almost all values of  $\omega$  and  $L$  we consider, indicating a Gaussian distribution of  $\mathcal{O}_{mn}$ .

As a further check that  $\mathcal{O}_{mn}$  obeys Gaussian distribution, we also calculate the the ratio  $\Sigma^2(n, \mu)$  [S6–S8] between the variances of diagonal and off-diagonal matrix elements for eigenstates in regions  $[n - \mu/2, n + \mu/2]$  of width  $\mu$ ,

$$\Sigma^2(n, \mu) = \frac{\sigma_d^2(n, \mu)}{\sigma_{od}^2(n, \mu)}. \quad (\text{S21})$$

Here  $\sigma_d^2(n, \mu)$  and  $\sigma_{od}^2(n, \mu)$  are the variance of the diagonal and off-diagonal matrix elements of the corresponding submatrices considered here (see also [S1]). In Figs. S4 (a) and S4 (b), we study the ratio  $\Sigma^2(n, \mu)$  of operator  $\mathcal{A}$  for  $q = 1$  and  $q = L/2$ , respectively. Specifically, the data are obtained for  $L = 16$  with two different square sizes  $\mu = 100, 1000$  and all possible embedding along the diagonal of the submatrix with dimension  $\mathcal{D}' \approx \mathcal{D}/2$ , where  $\mathcal{D}$  is the total dimension of the Hilbert space. For all cases we consider here,  $\Sigma^2(n, \mu)$  fluctuates around the GOE prediction  $\Sigma_{GOE}^2 = 2$ .

Furthermore, Figs. S4 (c) and S4 (d) show the averaged

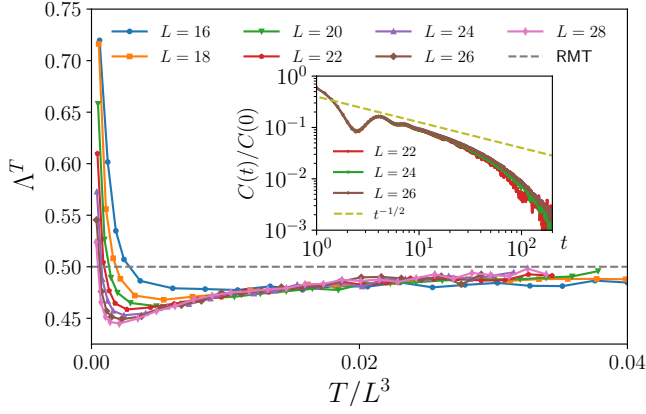


FIG. S6.  $\Lambda^T$  versus  $T/\tau_{\text{th}}$  for local operator  $\mathcal{A}_L$  in XXZ model (described by  $\mathcal{H}_3$ ). Data for  $L = 16$  is obtained by exact diagonalization, while data for  $L \geq 18$  is obtained by our typicality approach, averaged over  $500 \times (\frac{18}{L})^2$  states. The dashed horizontal line indicates the RMT value  $\Lambda^T = 0.5$ . The inset shows the autocorrelation function  $C(t) = \text{Tr}[\mathcal{A}_L(t)\mathcal{A}_L]/2^L$ , normalized by its initial value, where the dashed line indicates a  $\propto t^{-1/2}$  decay.

value

$$\overline{\Sigma^2(\mu)} = \frac{1}{\mathcal{D}' - \mu} \sum_{n=1+\mu/2}^{\mathcal{D}' - \mu/2} \Sigma^2(n, \mu). \quad (\text{S22})$$

We find that  $\overline{\Sigma^2(\mu)} \approx \Sigma_{\text{GOE}}^2$  for small  $\mu$ , while it grows monotonously with increasing  $\mu$  (this growth is particularly pronounced in the case of slowest mode  $q = 1$  as shown in Fig. S4 (c)). Comparing the results for different  $L$ , we find that  $\overline{\Sigma^2(\mu)}$  remains closer to  $\Sigma_{\text{GOE}}^2$  for larger  $L$ , and it is reasonable to expect that  $\overline{\Sigma^2(\mu)} \approx \Sigma_{\text{GOE}}^2$  holds in the thermodynamic limit  $L \rightarrow \infty$ , indicating  $\mathcal{O}_{mn}$  follow a Gaussian distribution, at least for  $m, n$  in the middle of the energy spectrum.

## NUMERICAL RESULTS OF $\Lambda^T$ FOR XXZ MODEL

In addition to the Ising model studied in the main text, we also consider a XXZ model,

$$\mathcal{H}_2 = \sum_{\ell=1}^L s_x^\ell s_x^{\ell+1} + s_y^\ell s_y^{\ell+1} + \Delta_1 s_z^\ell s_z^{\ell+1} + \sum_{\ell=1}^L \Delta_2 s_z^\ell s_z^{\ell+2} + h_1 s_z^1 + h_{\lfloor \frac{L}{3} \rfloor} s_z^{\lfloor \frac{L}{3} \rfloor}, \quad (\text{S23})$$

where  $s_{x,y,z}^\ell = \frac{1}{2} \sigma_{x,y,z}^\ell$  are spin operators at lattice site  $\ell$ ,  $L$  is the length of the chain with periodic boundaries, and we choose  $\Delta_1 = 1.5, \Delta_2 = 0.5, h_1 = 0.1, h_{\lfloor \frac{L}{3} \rfloor} = 0.075$  ( $\lfloor \cdot \rfloor$  indicates the floor function). The two defects are added to lift the translation and reflection symmetries. The zero magnetization subspace is considered and the energy

center is chosen to be  $E_0 = -0.3L/16$ , corresponding to infinite temperature. We consider a spin density-wave operator,

$$\mathcal{A}_s = \sum_{\ell=1}^L \cos\left(\frac{2\pi}{L} \ell q\right) s_z^\ell, \quad (\text{S24})$$

which exhibits slow hydrodynamics relaxation in the limit of small  $q$ .

In Fig. S5, analogous to the results of Ising model, we find that the onset of strict RMT behavior may only occur at much longer times  $T_{\text{RMT}} \geq \tau_{\text{th}}$ . Similarly, by plotting  $\Lambda^T$  as a function of  $T/(\tau_{\text{th}}L)$ , see inset of Fig. S5 (a), a good numerical collapse extending through almost all values of  $T$  can be observed for the density wave operator  $\mathcal{A}_s$  with ( $q = L/2$ ), which tentatively suggests  $T_{\text{RMT}} \propto \tau_{\text{th}}L$  for this operator. The collapse is not as clear for  $q = 1$ , see inset of Fig. S5 (b).

Moreover, as a comparison with the results in Ref. [S1], we also consider a model used there,

$$\mathcal{H}_3 = \sum_{\ell=1}^L s_x^\ell s_x^{\ell+1} + s_y^\ell s_y^{\ell+1} + \Delta_1 s_z^\ell s_z^{\ell+1} + \sum_{\ell=1}^L \Delta_2 s_z^\ell s_z^{\ell+2} + h_1 s_z^1 + h_{\lfloor \frac{L}{2} \rfloor} s_z^{\lfloor \frac{L}{2} \rfloor}, \quad (\text{S25})$$

and a local operator  $\mathcal{A}_L = s_z^{\lfloor \frac{L}{2} \rfloor}$  in the middle of the chain, which exhibits a power-law relaxation. We choose the same parameters  $h_1 = 0.1, h_{\lfloor \frac{L}{2} \rfloor} = 1, \Delta_1 = 1.5, \Delta_2 = 1.2$ , open boundary conditions and consider the zero magnetization subspace. As shown in in Fig. S6, we find that although a “sharp transition” to RMT seems to exist for small system sizes ( $L = 16$ ), the analysis of longer chains unveils that strict RMT behavior may only occur at times much longer than the thermalization time. Interestingly, we observe a good numerical collapse of all the curves as a function of  $T/L^3$ , which coincides with the analytical prediction in Ref. [S4].

\* jiaozi.wang@uos.de

† jgemmer@uos.de

- [S1] J. Richter, A. Dymarsky, R. Steinigeweg, and J. Gemmer, Phys. Rev. E **102**, 042127 (2020).  
[S2] F. Jin, D. Willsch, M. Willsch, H. Lagemann, K. Michielsen, and H. De Raedt, J. Phys. Soc. Jpn. **90**, 012001 (2021).  
[S3] T. Heitmann, J. Richter, D. Schubert, and R. Steinigeweg, Z. Naturforsch. A **75**, 421 (2020).  
[S4] A. Dymarsky, arXiv:1804.08626.  
[S5] T. LeBlond, K. Mallayya, L. Vidmar, and M. Rigol, Phys. Rev. E **100**, 062134 (2019).  
[S6] L. D’Alessio, Y. Kafri, A. Polkovnikov, and M. Rigol, Adv. Phys. **65**, 239 (2016).

- [S7] R. Mondaini and M. Rigol, Phys. Rev. E **96**, 012157 (2017).
- [S8] D. Jansen, J. Stolpp, L. Vidmar, and F. Heidrich-Meisner, Phys. Rev. B **99**, 155130 (2019).
- [S9] M. Brenes, S. Pappalardi, M. T. Mitchison, J. Goold, and A. Silva arXiv:2103.01161.